

# A Interface Formation in Two-Phase Flow Problems

K. Fraňa and I. Nová

*Abstract*—the objective of the paper is a numerical investigation of the multi-phase unsteady flow problem representing the formation and kinetic of bubbles. The mathematical model is given by the equation system used commonly for the three-dimensional viscous unsteady laminar flow problem. Shapes and forms of the phase-interface between gas-liquid depend strongly on the used grid resolution. Generally for various grid resolutions, different bubble formations were found. However, the volumetric fraction of the gas in the mixture was identical up to particular time. In advanced time, different progress of the gas decomposition was identified and the gas amount in the mixture was significantly lower in respect to the theoretical assumption. Furthermore, kinetic and bubble formations were investigated in liquids with various kinematic viscosity. It was found that kinematic viscosity could evidently influence the bubble formation, size and shape, but not a capability of the liquid to capture gas in the liquid as it can be assumed.

*Keywords*— bubble formation, grid study, numerical simulation, unsteady.

## I. INTRODUCTION

THE material property e.g. a specific weight is an important subject of the light constructions. In case of the light construction, the fuel consumption can be significantly reduced. In last decades composite materials are mostly preferred because of the reduced weight. However, there are still a lot of technical applications, where the metal based materials are preferred from much advantageous e.g. sufficient resistance on the higher temperature. The cellular material structures are providing the reduced specific weight of the metal based products as well and provides simultaneously the higher temperature resistance.

In generally, it can be found many production technologies to obtain the cellular type structures e.g. the continuous gas injection in the melted materials containing mostly other stabilization components. Stabilization components in melts lead to the increase of the mixture viscosity. Details about

cellular material production can be found in [1] or [4]. If the gas is directly injected into the melt, this method is called as the direct foaming. The production of the AL-foams using stabilization articles based on the components SiC or MgO has been already successfully applied at the industrial scale as was demonstrated in [5] or [6]. The method of the direct foaming is generally simple, however, requires a present of the small particles of the  $\mu\text{m}$  size supporting the stabilization of the foaming process. However, these small particles, required for a foam production, prevent later the recycling of these cellular material structures. From the point of the physics and melt mixture properties, it was found the small particles in melts increase the kinematic viscosity of the fluids [9]. Regardless of the type and geometry of the particles, the viscosity value increased with an increased amount of particles. For instance, the effect of the small different particles on the viscosity increase was studied in water in [8]. In the case of rough MgO particles, a smaller diameter particle leads to sufficient viscosity using a lesser amount of material. This tendency can be confirmed in the case of rough  $\text{Al}_2\text{O}_3$  (size varies from 1.0 to 3.0  $\mu\text{m}$ ) and sphere  $\text{SiO}_2$  (size varies from 0.9 to 8.0  $\mu\text{m}$ ). Therefore, smaller particles have the advantage of increasing the viscosity of the suspension under identical particle geometry and type. However, to obtain similar viscosity values, more additive is required, if the geometry different but the particles are the same [7].

This paper addresses a problem of the two-phase laminar unsteady mixture flow of the aluminum melt and gas simulated using the numerical approach. Experimentally it was found basic facts about the fluid viscosity changed due to small particles in the suspension. The numerical study is based on this assumption of the small particle behavior in mixture and focuses on the prediction of bubbles formation under various viscosity magnitudes. The flow problem of the gas-liquid mixture can be found not only in the material production, but in many other applications. The gas-liquid two-phase flow within a double inlet cyclone for natural gas separation was numerically simulated using the discrete phase model e.g. in [9]. The numerical approach was validated with the experimental data, and the comparison results agreed well with each other. A newly developed computational fluid dynamics (CFD) model based on a multi-phase particle method was presented in [2] for predicting the entrainment behavior of liquid metal into slag due to rising single bubble. The other example representing a calculation of the dispersed water wave as a compressible mixture of air and water with

This work was supported by the Ministry of Education, Youth and Sports of the Czech Republic and the European Union - European Structural and Investment Funds in the frames of Operational Programme Research, Development and Education - project Hybrid Materials for Hierarchical Structures (HyHi, Reg. No. CZ.02.1.01/0.0/0.0/16\_019/0000843).

K. Fraňa is with the Technical University of Liberec, Faculty of Mechanical Engineering, Department of Power Equipment, Studentska 2, 46117, Liberec, Czech republic (corresponding author to provide phone:+420 485353436; e-mail: karel.frana@tul.cz).

I. Nová is with the Technical University of Liberec, Faculty of Mechanical Engineering, Department of Engineering Technology, Studentska 2, 46117, Liberec, Czech republic (e-mail: iva.nova@tul.cz).

homogeneous material properties was examined in [13] or in [16]. The two-phase flow in a porous material was investigated using VOF in [14]. The corresponding mathematical equations were based on a multiphase flow model which was built on the conservation laws of mass, momentum and energy as well as the gas-phase volume fraction advection equation. This similar equation model was adopted in the present paper as well. The two-phase problem with porous materials examined by numerics was introduced in [15]. The two-phase flow over two types of step-poolspill was successfully investigated using two-phase schemes VOF and with various turbulence modeling in [9]. The VOF approach was sufficiently used in [18] as well.

The following paper text is organized as follows. Section 2 introduces the investigated problem, describes a computational domain and techniques used for a numerical simulation. Basic theoretical knowledge about a bubble formation is presented as well. Section 3 contains results of the simulation and demonstrates a feasibility of the used calculation solver for the problem of the two-phase mixture simulation. Section 4 discusses main conclusions about two-phase flow result discovered due to numerical simulations

## II. PROBLEM FORMULATION

### A. Material mixture

The investigated problem is described by a multi-phase flow representing a liquid-gas mixture system. The liquid phase is represented by the aluminum melt and it is defined in numerical simulation as a perfect fluid. Because the change of the temperature in the aluminum melt is relatively small, the

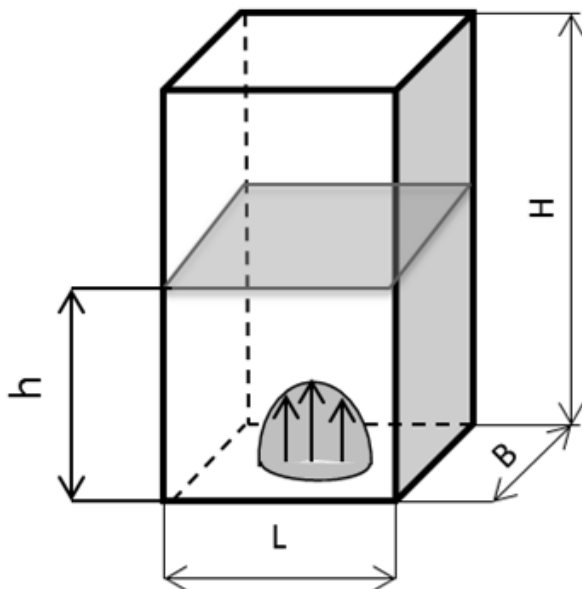


Fig. 1 sketch of the computational domain with boundaries

density remains to be mostly constant value. The second phase is air and it is considered as an ideal gas. In case of the different material properties the multiphase approach was

used. The each component  $n$  of the mixture is considered to be compressible and non-isothermal immiscible fluid.

### B. Computational domain

The computational domain (see in Fig. 2) is in a form of the box  $L \times B \times H$  with a size of  $0.4\text{m} \times 0.4\text{m} \times 1\text{m}$ . The periodic boundary conditions are applied on all side walls. The inlet/outlet boundary type condition is prescribed for the top of a box having zero values for all phases except the phase air for which the input/output velocity magnitudes are calculated. For the bottom of the air phase, the parabolic inlet velocity profile is defined. The peak velocity of the jet is constant of  $0.084\text{ m/s}$  or varying (if the intensity of the bubble formation is an objective of examination).

### C. Mesh

The computational mesh has a spacing of  $100 \times 100 \times 120$  resulting 1.28 million hexahedral type cells. This relatively fine mesh was used for numerical investigation of the flow problem. However, for the grid study, various grid spacing meshes were tested in order to find a grid dependency e.g. 1.15 million cells and 0.96 mill. cells respectively.

## III. MATHEMATICAL MODEL

To solve the phase interface interaction, the volume of fluid approach (VOF) [12], [10] and [17]. based on the interface capturing methods was applied. The migration of gas bubbles immersed in a liquid under the action of temperature gradient and surface tension (Marangoni flow) in zero gravity environment was numerically investigated in [8]. Details about surface tension applied for a calculation can be found in [3]. Generally, the material properties of the homogeneous mixture are described by the volume fraction function for the phase 1, 2 and more. In case of the two-phase flow problem considered in this study, the volume fraction  $\alpha_1$  represents a liquid and  $\alpha_2$  is a gas. The mathematical model used for the flow of the two-phase mixture consists of the mass, momentum and energy conservation laws. A conservation law of mass for each component separately must be also included. Furthermore, gravitational effects should be considered and included for liquid-phase wave problems as well. Finally, the underlying conservative part of the flow model can be expressed in (1).

$$\frac{\partial \bar{U}}{\partial t} + \frac{\partial \bar{F}_1}{\partial x} + \frac{\partial \bar{F}_2}{\partial y} + \frac{\partial \bar{F}_3}{\partial z} = \bar{G} \quad (1)$$

$\bar{U}$  is the vector of conservative variables,  $\bar{F}$  is the flux function, and  $\bar{G}$  are the source terms and these terms are defined as in (2).

$$\bar{U} = \begin{bmatrix} \alpha_1 \rho \\ \alpha_2 \rho \\ \rho u \\ \rho v \\ \rho w \\ \rho e \end{bmatrix}, \quad \bar{F}_1 = \begin{bmatrix} \alpha_1 \rho u \\ \alpha_2 \rho u \\ \rho u^2 + p - \tau_{xx} \\ \rho v u - \tau_{xy} \\ \rho w u - \tau_{xz} \\ \rho h u - u \tau_{xx} - v \tau_{xy} - w \tau_{xz} + q_x \end{bmatrix},$$

$$\bar{F}_2 = \begin{bmatrix} \alpha_1 \rho v \\ \alpha_2 \rho v \\ \rho uv - \tau_{yx} \\ \rho v^2 + p - \tau_{yy} \\ \rho wv - \tau_{yz} \\ \rho hv - u\tau_{yx} - v\tau_{yy} - \tau_{yz} + q_y \end{bmatrix}$$

$$\bar{F}_3 = \begin{bmatrix} \alpha_1 \rho w \\ \alpha_2 \rho w \\ \rho uw - \tau_{zx} \\ \rho vw - \tau_{zy} \\ \rho w^2 + p - \tau_{zz} \\ \rho hu - u\tau_{zx} - v\tau_{zy} - \tau_{zz} + q_z \end{bmatrix}, \text{ and } \bar{G} = \begin{bmatrix} 0 \\ 0 \\ 0 \\ 0 \\ -\rho g \\ \rho hv \end{bmatrix} \quad (2)$$

The velocity components  $u$ ,  $v$  and  $w$  are calculated by (2) along the  $x$ ,  $y$  and  $z$  axes,  $g$  is the gravitational acceleration,  $p$  is pressure,  $\tau$  is a component of the Reynolds stress tensor,  $e$  is inertial energy and  $h$  is the enthalpy given in (3).

$$h = \frac{\rho e + p}{\rho} \quad (3)$$

For initialization process the phase volume fraction  $\alpha_1$  must prescribed as a value of 1 for the entire domain defined by the high of the container of 0.52 m. The space above this aluminum melt represents air with  $\alpha_2$  to be 0 (the rest of the cube container). This initial boundary prescription is common for a typically two-phase concept of solution. The calculation was carried out in OpenFOAM code using PIMPLE scheme. The Gauss linear scheme was applied for the most of all variables. The compressible Multiphase solver was used with varied time step determined by the stability condition based on the maximal Courant number of 0.25.

#### IV. PROPERTIES OF BUBBLES

To predict a behavior of the bubbles, Reynolds number ( $Re$ ) defined in (7) is commonly used together with Weber number ( $We$ ) or Haberman-Morton number. The intensity of the fluid stress influences a deformation of the bubbles which is the characteristic force maintaining the sphericity of the bubble. It is known from theory that bubble deformation will occur when  $We/Re$  approaches unity for  $Re \ll 1$  or when  $We$  approaches unity for  $Re \gg 1$ . This Reynolds number is defined as follows

$$Re = \frac{2 \rho w R}{\mu_c}, \quad (7)$$

where  $R$  is the instantaneous radius of the spherical bubble,  $w$  is a magnitude of the translational velocity,  $\mu_c$  and  $\rho$  are the kinematic viscosity and density respectively. The Weber number is given by (8).

$$We = \frac{2 \rho_A w_\infty^2 R}{S} \quad (8)$$

The term  $w_\infty$  is a terminal velocity and  $S$  is a surface friction. The effect of the Weber number on the bubble formation can be found e.g. in [19]. Terminal velocity is a function of shape and to calculate the Weber number, this value must be known. According to [13], this velocity can be replaced by the  $\Delta w$

which expresses the relative gas-liquid velocity. Generation of small-scale dynamics has to take into account the ratio of the hydrodynamic force related to dynamic pressure, to the force of surface tension. This is expressed in fluid mechanics by the Weber number. The hydrodynamic force is conveniently defined as  $\rho \Delta w^2$ , so that it captures both the case of a high gas velocity over slow liquid and a high velocity liquid jet in a static gas, breaking into droplets. Depending on the local shape, breakup of the bubble can occur above some critical value of  $We$ . Below this value, the surface tension forces are large enough to overcome the dynamic pressure, and there is

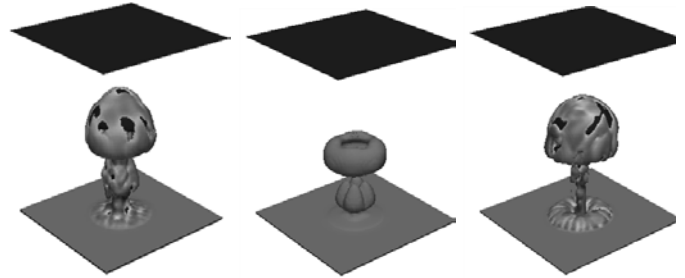


Fig. 2 formation of the phase interface for grids 75%, 90% and 100% for the time 0.6s

no local breakup. At larger Weber numbers, the domination of the aerodynamic force leads to distortion and spray. This process creates small bubbles with a smaller Weber number. Their size is small enough, they drop below the critical level and the breakup process stops. Another option for a prediction of the bubble behavior is to express the Haberman-Morton number (see (9)).

$$Hm = \frac{g \mu_A^4}{\rho_A S^3} \quad (9)$$

In this case if  $Hm < 1$  all bubbles for which  $Re \ll 1$  will remain spherical. However, there are some unusual circumstances in which  $Hm > 1$  and then there will be a range of  $Re$  in which significant departure from sphericity might occur [11]. For the assumed problem of the two-phase flow, it was calculated that  $Re \gg 1$  and will be approx.. of  $Hm = 3 \times 10^{10}$ . In this particular case, the terminal velocity is given by the Froude number  $Fr \approx O(1)$  and distortion will occur if  $We > 1$ .

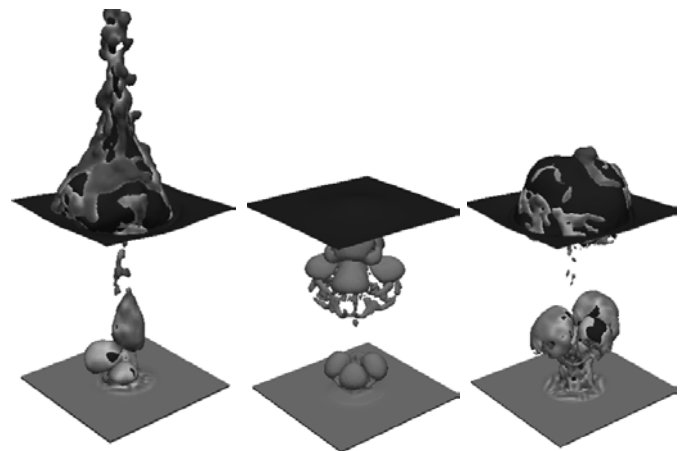


Fig. 3 formation of the phase interface for grids 75%, 90% and 100% and for the time step 1s

Using  $Fr = 1$  and  $Hm$  it follows that departure from sphericity will occur when  $Re \gg Hm^{-1/4}$ . Consequently, in the common circumstances in which  $Hm < 1$ , there exists a range of Reynolds numbers,  $Re < Hm^{-1/4}$ , in which sphericity is maintained; non-spherical shapes occur when  $Re > Hm^{-1/4}$ . Experimentally, it is observed that the initial departure from sphericity causes ellipsoidal bubbles that may oscillate in shape and have oscillatory trajectories. As the bubble size is further increased to the point at which  $We \approx 20$ , the bubble acquires a new asymptotic shape, known as a spherical-cap bubble [11].

## V. RESULTS

### A. Grid study

It can be assumed, the gas distribution of the two-phase

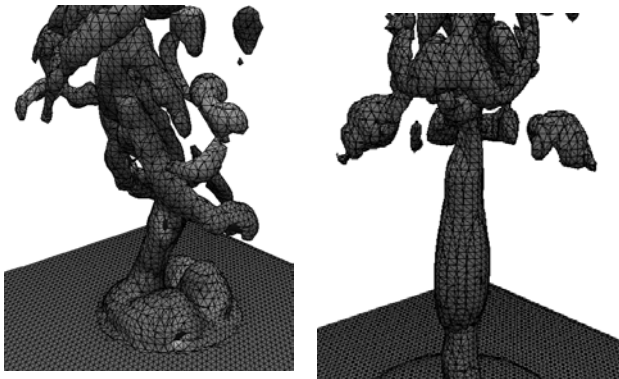


Fig. 4 detailed formation of the phase interface for grids 75%, and 90% for the time 1,5s

system in the computational domain can be influenced by the applied grid resolution. In order to identify this effect of the grid resolution on the gas decomposition amount a grid study

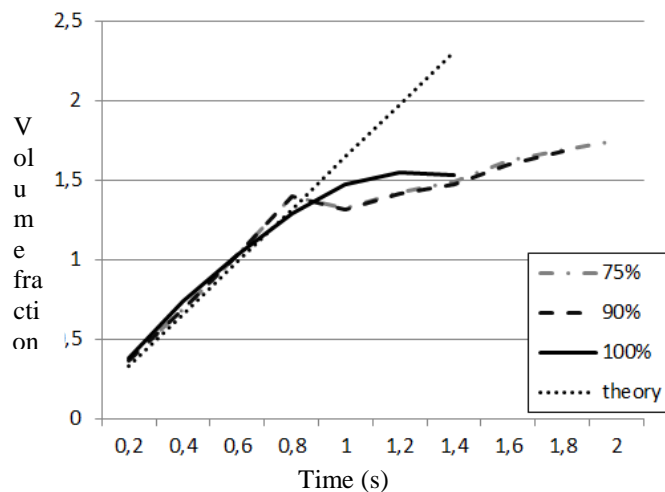


Fig. 5 volume fraction of the gas deposition in time

was carry out. Three different grids defined by the total number of the cells were generated. The grid denoted by 100 % consisted of 1.28 mill. tetrahedral cells and it is called as an original grid or reference grid. The grid denoted by 90%

contained about 10 % less cells than the original one. Finally the grid denoted as 75% contain about 25% less cells. Fig. 2 shows a formation of the phase interface between air and metal liquid for the time period 0.6s after the simulation start. The particular form of the bubble characteristic for the particular time can be observed. Results obtained confirmed the grid resolution had a strong impact on the onset of bubbles in respect to the shape and form, especially for the grid resolution given by 90% of cells. Fig. 3 depicts the same results, however, for the advanced time 1s. Whereas the results provided on the grid resolution 90% were completely different, the results from the grid 75% and 100% demonstrated a fluid jet above the phase level. In case of the grid resolution given by 75%, this jet flow was significantly stronger than the jet founded for the grid 100%. Therefore, it was found that the grid resolution influenced not only the formation of bubbles, but the flow features in the area of the gas phase (above the fluid level).

If the original grid resolution was used, the jet of the bubble form was created above the liquid level, as well. However, its high was evidently damped. In case of the grid 90%, the formatted bubbles were still under the liquid level. The results for the time 0.6s or 1s calculated on the grid 90% demonstrated so kind of the “delay” during the formation of the flow. Therefore, the grid resolution influenced not only the forms of the bubbles, but the intensity of the bubble formation as well. Fig. 4 shows the particular form the phase interface and grids. Mostly, the grid was enough fine to capture a complex shape of the phase interface. Even for advanced time, the significant differences in the bubble formation are still possible to see.

Fig. 5 illustrates a progress of the volume gas deposition in the mixture in time. Grids defined by 75% or 90% of the original grid provided the similar behavior of the gas. Up to 0.8 s, the linear increase of the gas was observed, however,

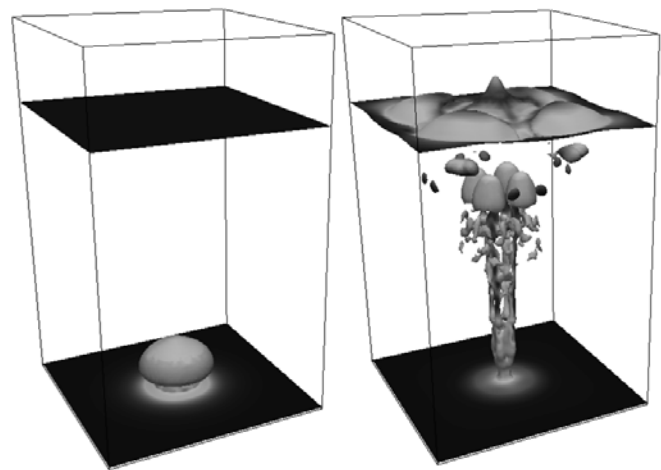


Fig. 6 instantaneous bubble patterns for the time (a) 0.3s and (d) 1.2s

about 1s, the increase of the gas contain was not so intensive. In case of the reference grid, up to 0.8s the gas deposition is similar as in the previous results; however, later significant differences were visible. The gas contain was increasing up to

1s and after that it began to decline. As a reference, the point line given by a theory calculation is indicated which demonstrates the increase of the gas deposition based on the continuous inlet boundary condition. The inlet condition characterized by the inlet velocity and diameter of the gas jet were described already in chapter II. The gas spread depicted by the volume fraction was calculated to be 1.6485 % per second. Under assumption, that the inlet condition would be constant, each second the volume fraction of the gas will be increased by 1.6485 %. As it is shown in Fig. 5, real gas deposition in the computational domain was in a good match to the theoretically calculated values only up to the time of 0.8s. After that, the result deviation was systematically increasing.

*B. A formation of the bubble path for the kinematic viscosity of the liquid phase 0.014 Pa.s*

Figure 6 shows an instantaneous flow pattern of the bubble formation for different time steps: 0.3 and 1.2s, respectively. For further calculation, the original computational grid denoted as 100% resolution was used. Firstly, to find a behavior of the bubble formation, the dynamic viscosity of the liquid (aluminum melt) was constant of 0.014 Pa.s. The gray scale depiction (from white to black color) in Fig. 6 indicates the intensity of the flow velocity. It was observed the first bursting of the main bubble and other small bubbles remain entrained in the fluid, floating slowly to the surface. The first bubble was breakup into other small bubbles and this process continued during floating of the bubbles to the surface of the mixture. In Fig. 6 for the time 1.2s, the path of the different

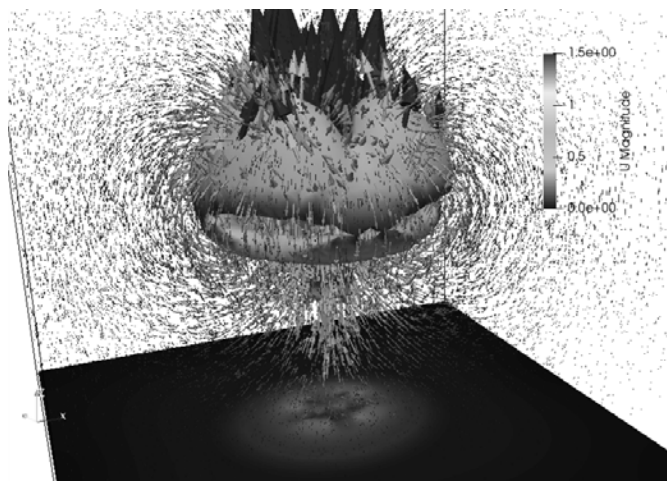


Fig. 7 formation of the bubbles with velocity vectors at the time 0.55s.

size bubbles between bottom and surface of the aluminum melt (liquid form) was observed. The smaller bubbles created later, after the first bursting, reached the higher velocity (indicated by the bright color). The liquid surface was deformed by the incoming bubbles.

Due to this movement, the bubble is deformed from the spherical form (still possible to see it in Fig. 6 for the time 0.35s). Around the bubble, there is a significant flow taking the mass from the upper part of the bubble to the lower part

which is later pump throughout the center of the bubble again. This flow exists because of the translational movement of the bubble how the liquid past the form the bubble body. Different flow past a bubble was examined in [15].

Figure 5 shows a first main bubble in time of 0.55s. The vector depiction indicates a flow orientation and the intensity of the velocity. It was detected that in the center of the bubble, there is the highest velocity taking a value up to 1.5 m/s. This intensive translation velocity is approx. 180 times higher than the initial air velocity used for a first creation of the bubble at the bottom.

Figure 6 illustrates the temperature distribution in the two-phase mixture in the time 1.15s. At the bottom of the container, the slight heat flux was set up which is caused the cooling effect of the bottom and therefore, the resulting temperature is lower about 719.6 K. The circulating surrounding air has the temperature of 295 K (area above the aluminum surface). At this surface, the cooling effect of the surrounding air is considered leading to the significant drop of the temperature. The air flow above the aluminum level is driven by a buoyancy force due to the strong temperature gradient. Inside of the aluminum melt, the temperature is homogenous around 720 K. The effect of the temperature was

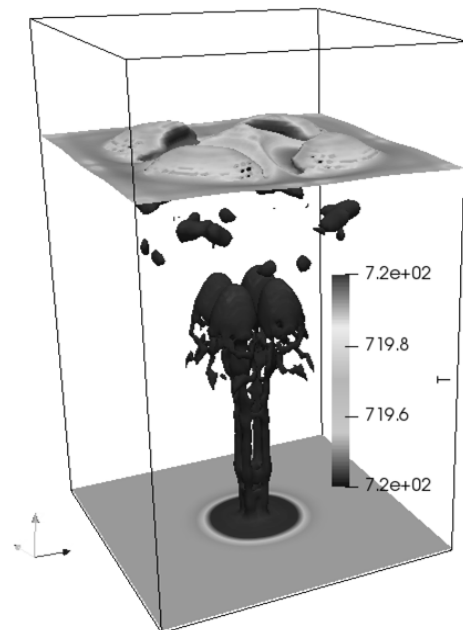


Fig. 8 instantaneous temperature field in time 1.15s.

taken into account for the calculation because of the existence of the slight temperature gradient between bottom and top of the container. Generally, this existing temperature gradient may cause a flow of the aluminum melt driven by a buoyancy force which influences the total bubble motion as well. From the point of the forces acting on the bubble at small relative Reynolds number  $Re \ll 1$ , only the forces due to buoyancy and the weight of the particle need be consider to the total force acting on the bubble. However, at high relative Reynolds numbers,  $Re \gg 1$ , one must resort to a more heuristic approach in which the fluid forces are supplemented by drag

(and lift) forces [15].

### C. An Influence of the viscosity on the bubble path formation

Several different viscosities of the liquid phase starting from 0.014 Pa.s to 0.28 Pa.s were assumed for a study on the bubble formation. It was found experimentally in previous experimental studies and already discussed above, to produce the metal foam in the liquid phase; the stabilization effect must be established due to the small particles of different size.

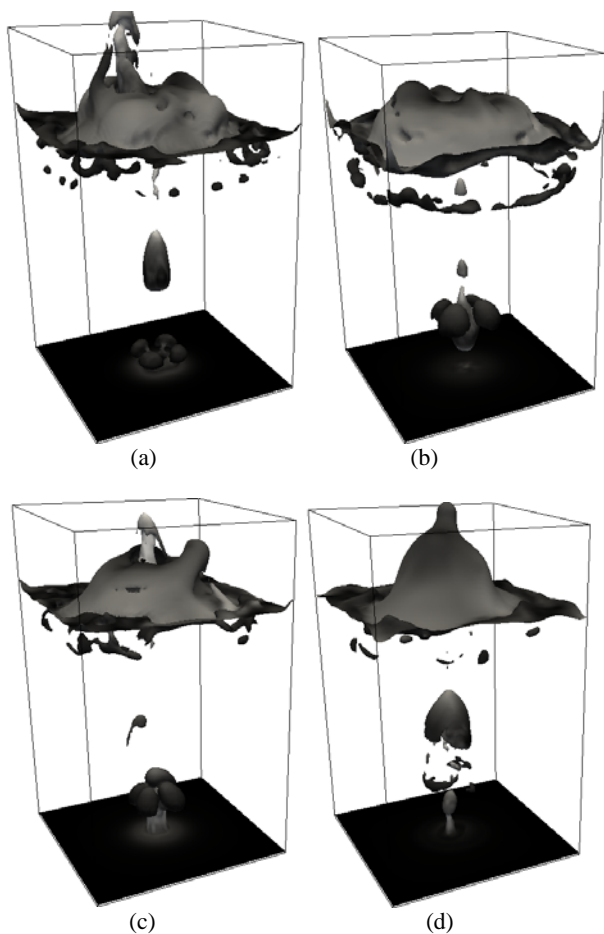


Fig. 9 instantaneous contours of the gas volume fraction in time 1.6s for the dynamic viscosity: (a) 0.014 Pa.s, (b) 0.07 Pa.s, (c) 0.14 Pa.s, and (d) 0.28 Pa.s.

Small particles caused a slightly higher fluid viscosity. To assume these small particles in the simulation would be to complex, therefore, the effect of the small particles was replaced by the change of the fluid viscosity (as it was experimentally observed as a consequence of the small particles). Fig. 9 shows a gas volume fraction in the liquid phase for the time 1.6s and for different viscosities starting from 0.014 Pa.s up to 0.28 Pa.s, respectively. For the smaller time, the higher viscosity had an effect of the bubble formation in sense that a shape of the bubble was modified. Later, the fluid kinematic viscosity influenced the shape and form of the gas-liquid interface. Unfortunately, higher viscosity did not lead to the formation of the foam. It

influenced only the bubble formation and gas deposition amount in the liquid. This fact has already been observed in the grid study in Fig. 5.

## VI. CONCLUSION

The bubble formation in the mixture represents the typical two-phase problem which was investigated by means of numerical simulations. The flow problem was considered to be unsteady, laminar and non-isothermal. The influence of the kinematic viscosity of the liquid fluid on the formation of the bubble path was studied in details. The compressible multi-phase solver of the OpenFOAM computational code was successfully applied for this problem. It is evident that the preferred solver provided reasonable results which can be expected based on the fluid mechanics knowledge. The grid study revealed a complex system of the parameters having an influence of the gas decomposition in the liquid phase. It is not only the problem of the gas decomposition in a liquid phase, but the shape and kinetics of the formed bubbles as well. Up to the particular time step, the progress of the gas decomposition in the liquid was identical and therefore independent on the grid resolution. In advanced progress, the deviation between results became to be evident.

Furthermore, it was found that the fluid kinematic viscosity influenced the formation of the bubbles (shape and total volume fraction of the gas in the mixture). However, this effect of the viscosity on the formed bubbles could not be unambiguously confirmed. The further calculation will be needed to determine, which particular material properties or flow conditions can stabilize really the foam and prevent a leak of the gas from the mixture. It is evident that only the material property like kinematic viscosity can not sufficiently contribute to the foam formation. Moreover, from the point of the calculation effectiveness, the higher velocity magnitudes appeared above the aluminum melt in the region of the air flow. Unfortunately, these higher velocity values determine the time step size and therefore the requirement of the total time for a calculation.

## ACKNOWLEDGMENT

Authors thanks to the Ministry of Education, Youth and Sports of the Czech Republic and the European Union - European Structural and Investment Funds in the frames of Operational Programme Research, Development and Education - project Hybrid Materials for Hierarchical Structures (HyHi, Reg. No. CZ.02.1.01/0.0/0.0/16\_019/0000843).

## REFERENCES

- [1] D. K. Rajak, L.A. Kumaraswamidhas1 and S. Das, "Technical Overview of Aluminum Alloy Foam," *Material Science* 48, 2007, pp. 68-86.
- [2] S. Natsui, H. Takai, T. Kumagai, T. Kikuchi and R. O. Suzuki, "Multiphase Particle Simulation of Gas Bubble Passing Through Liquid/Liquid Interfaces," *Materials Transactions*, Vol. 55, No. 11 (2014) pp. 1707-1715.
- [3] H.C. Kuhlmann, *Thermocapillary Convection in Models of Crystal Growth*, 152, Springer, Berlin, Heidelberg (1999) Springer Tracts in Modern Physics.

- [4] R. Goodall and A. Mortensen, *Porous Metals, in Physical Metallurgy*, ed. D. E. Laughlin and K. Hono, Elsevier, Oxford, 5th edn, 2014, pp. 2399–2595, ch.4.
- [5] P. Åsholt, *Metal Foams and Porous Metal Structures*, ed. J. Banhart, M.F. Ashby, and N.A Fleck (Bremen, Germany: MIT-Verlag), 1999, pp. 133.
- [6] J. Wood, *Metal Foams*, ed. J. Banhart and H. Eifert (Bremen, Germany: MIT-Verlag), 1997, pp. 31.
- [7] J. Banhart, “Manufacturing Routes for Metallic Foams,” *Solidification Science: Over view Journal JOM* vol. 52, no.12, 2000, pp. 22-27.
- [8] K. Kadoi and H. Nakae, “Relationship between Foam Stabilization and Physical Properties of Particles on Aluminum Foam Production,” *Materials Transactions*, vol. 52, no. 10, 2011, pp. 1912-1919.
- [9] Y. Yang, S. Wang and C. Wen, “Gas-liquid two-phase flows in double inlet cyclones for natural gas separation,” *Cogent Engineering*, 4(1), DOI: 10.1080/23311916.2017.1373421, 2017.
- [10] Y. Alhendala, A. Turana, and Wael I.A. Alyb, “VOF simulation of marangoni flow of gas bubbles in 2D-axisymmetric column,” *Procedia Computer Science*, Vol 1, Issue 1, 2010, pp. 673-680.
- [11] A.H.Nikseresht, N.Talebeydokhti and M.J.Rezaei, “Numerical simulation of two-phase flow on step-pool spillways,” *Scientia Iranica*. Vol. 20, Issue 2, 2013, pp. 222-230.
- [12] C. W. Hirt and B. D. Nichols, “Volume of Fluid (VOF) Method for the Dynamics of Free Boundaries,” *Journal of computational physics*, vol. 39, 1981, pp. 201-225.
- [13] Z. H. Ma, D. M. Causon, L. Qian, C. G. Mingham, H. B. Gu, P. Martínez Ferrer, “A compressible multiphase flow model for violent aerated wave impact problems,” *Proc. R. Soc. A* vol. 470, <http://dx.doi.org/10.1098/rspa.2014.0542>, 2017.
- [14] S. Pasquier, M. Quintard and Y. Davit, “Modeling two-phase flow of immiscible fluids in porous media: Buckley-Leverett theory with explicit coupling terms,” *Physical Review Fluids*, vol. 2, no. 10, 2017, pp. 104101/1-104101/19.
- [15] Ch. E. Brennen, *Fundamentals of the multiphase flow*, Cambridge University Press 2005.
- [16] L. Hružík, M. Vašina, and A. Bureček, “Evaluation of bulk modulus of oil system with hydraulic line,” *EPJ Web of Conferences*, EDP Sciences, 2013, Vol. 45, p. 01041.
- [17] Q. Peng, L. Gui and Z. Fan. “Numerical and experimental investigation of splashing oil flow in a hypoid gearbox,” *Engineering Applications of Computational Fluid Mechanics*, 12:1, DOI: 10.1080/19942060.2018.1432506, 2018, pp. 324-333.
- [18] A. Albadawi, D. B. Donoghue, A. J. Robinson, D. B. Murray and Y. M. C. Delauré, A. Albadawi, A. Albadawi, “On the assessment of a VOF based compressive interface capturing scheme for the analysis of bubble impact on and bounce from a flat horizontal surface,” *International Journal of Multiphase Flow*, Vol. 65, 2014, pp. 82-97.
- [19] George Strotos, Ilias Malgarinos, Nikos Nikolopoulos, Manolis Gavaises, “Predicting droplet deformation and breakup for moderate Weber numbers,” *International Journal of Multiphase Flow*, Vol. 85, 2016, pp. 96-109.